Theory of the scanning tunneling microscope: Xe on Ni and Al

N. Mingo, L. Jurczyszyn,* F. J. Garcia-Vidal,† and R. Saiz-Pardo
Departamento de Fisica de la Materia Condensada, Facultad de Ciencias, Universidad Autonoma de Madrid, E-28049 Madrid, Spain

P. L. de Andres
Instituto de Ciencia de Materiales (CSIC), Universidad Autonoma de Madrid, E-28049 Madrid, Spain

F. Flores
Departamento de Fisica de la Materia Condensada, Facultad de Ciencias, Universidad Autonoma de Madrid, E-28049 Madrid, Spain

S. Y. Wu
Department of Physics, University of Louisville, Louisville, Kentucky 40292

W. More
Departamento de Fisica de la Materia Condensada, Facultad de Ciencias, Universidad Autonoma de Madrid, E-28049 Madrid, Spain
(Received 27 September 1995; revised manuscript received 4 December 1995)

We present a theory for the scanning tunneling microscope (STM) current based on a Keldysh Green function formalism. In our formalism, we solve self-consistently an *ab initio* linear combination of atomic orbitals Hamiltonian within a local density formalism. Total energy calculations for xenon deposited on metal surfaces are performed to obtain the equilibrium position, and the Green functions needed to compute the current are obtained at the same time. Structural and nonstructural effects that can influence the correct interpretation of experimental STM results are studied. We find good agreement between our calculations and experimental images taken under highly controlled conditions, and we conclude that STM images should be analyzed by comparing iteratively the theory and the experiment, much in the same way as it is usually done for other surface sensitive techniques like low-energy electron diffraction, photoelectron diffraction, surface-extended x-ray-absorption fine structure spectroscopy, etc. [S0163-1829(96)01427-0]

I. INTRODUCTION

The real-space nature of the scanning tunneling microscope (STM) provides atomic resolution on a variety of surfaces with apparently very little theoretical effort. However, shortly after the invention of the STM it became clear that electronic effects were at least as important as pure structural effects,[1] and a theoretical interpretation of the experimental data is important if a safe procedure for analyzing the experimental data is required. To obtain a theoretical formalism realistic enough to allow direct comparison with experiments, several difficult points should be considered: (i) in many cases, experimental conditions are such that a strong interaction between the tip and the sample is unavoidable, so simple perturbation theory cannot be used, (ii) the tunneling current is intrinsically a nonequilibrium problem, (iii) it is difficult to control precisely the tip shape and composition, making it necessary to try several plausible models for the tip, and finally (iv) a good description of the electronic properties of the clean surface, the surface plus any adsorbate (the sample), and the scanning tip is important to mimic the real experiment. Here, we stress the special difficulty of describing the tip, as it is important to include in the same formulation its quasiatomic character (yielding atomic resolution) and the existence of a bulk reservoir of electrons, allowing a steady current to be established between the tip and the sample. In a way, all these ingredients imply an important departure from the naive, earlier idea for the STM as a direct structural tool, but the examples where these factors are crucial to a safe interpretation of STM images are accumulating.

II. A LCAO HAMILTONIAN FOR CALCULATING TUNNELING CURRENTS

The scanning tunneling microscope is intrinsically a nonequilibrium setup. Therefore the nonequilibrium Green function formalism developed by Keldysh[2] is most adequate to analyze, from a theoretical point of view, the experiments carried out with this technique. The Hamiltonian for the tip-sample system can be written as a sum of three terms; one describing the tip (T), another describing the sample (S) (note that the sample can be a clean surface or a system composed of a clean surface plus an adsorbate, as previously defined), and finally a term that takes into account the interaction between the tip and the sample:[3]

$$\hat{H}=\hat{H}_T+\hat{H}_S+\hat{H}_I. \tag{1}$$

The interaction between the tip and the sample is described via hopping processes. Therefore we write the term $\hat{H}_I$ coupling tip and sample orbitals as a function of a hopping matrix ($\hat{T}_{TS}$), and the different creation and annihilation vector operators associated with these orbitals ($\hat{c}_T^{\dagger},\hat{c}_T,\ \hat{c}_S^{\dagger},\hat{c}_S$):

$$\hat{H}_I=\sum_{\alpha j}\left[\hat{T}_{TS}(\alpha j)\hat{c}_T^{\dagger}(\alpha)\hat{c}_S(j)+\hat{T}_{ST}(j\alpha)\hat{c}_S^{\dagger}(j)\hat{c}_T(\alpha)\right] \tag{2}$$

where the sum runs over all the orbitals in the tip (α) and the sample (j).

When a steady state (defined by the applied bias) is reached, the total current between the tip and the sample is independent of time and can be written[4]

$$J=\frac{ie}{\hbar}\sum_{\alpha j}\left[\hat{T}_{TS}(\alpha j)\langle\hat{c}_T^{\dagger}(\alpha)\hat{c}_S(j)\rangle-\hat{T}_{ST}(j\alpha)\langle\hat{c}_S^{\dagger}(j)\hat{c}_T(\alpha)\rangle\right] \tag{3}$$

where the averaged quantities in Eq. (3) can be expressed in terms of the nonequilibrium Green functions $\hat{G}^{+-}$:[2]

$$\langle\hat{c}_S^{\dagger}(j)\hat{c}_T(\alpha)\rangle=\frac{1}{i}\hat{G}^{+-}_{T\alpha,Sj}(t,t+0^+)=\frac{1}{2\pi i}\int_{-\infty}^{\infty}\hat{G}^{+-}_{T\alpha,Sj}(\omega)d\omega, \tag{4}$$

$$\langle\hat{c}_T^{\dagger}(\alpha)\hat{c}_S(j)\rangle=\frac{1}{i}\hat{G}^{+-}_{Sj,T\alpha}(t,t+0^+)=\frac{1}{2\pi i}\int_{-\infty}^{\infty}\hat{G}^{+-}_{Sj,T\alpha}(\omega)d\omega. \tag{5}$$

The last two expressions allow us to write the total current J as a function of the nonequilibrium Green functions:

$$J=\frac{e}{\pi\hbar}\sum_{\alpha j}\int_{-\infty}^{\infty}\left[\hat{T}_{TS}(\alpha,j)\hat{G}^{+-}_{Sj,T\alpha}(\omega)-\hat{T}_{ST}(j,\alpha)\hat{G}^{+-}_{T\alpha,Sj}(\omega)\right]d\omega. \tag{6}$$

This formula is readily simplified using well-known properties of the trace:

$$J=\frac{e}{\pi\hbar}\int_{-\infty}^{\infty}\mathrm{Tr}\left[\hat{T}_{TS}\hat{G}^{+-}_{ST}(\omega)-\hat{T}_{ST}\hat{G}^{+-}_{TS}(\omega)\right]d\omega. \tag{7}$$

The nonequilibrium Green functions that appear in the expression of the current can be related to the *equilibrium* retarded and advanced Green functions of the interacting system, $\hat{G}^R$ and $\hat{G}^A$, using the following Dyson-like equation for nonequilibrium Green functions:[2]

$$\hat{G}^{+-}(\omega)=[\hat{I}+\hat{G}^R(\omega)\hat{\Sigma}]\hat{g}^{+-}(\omega)[\hat{I}+\hat{\Sigma}\hat{G}^A(\omega)], \tag{8}$$

where $\hat{\Sigma}$ yields the interaction between the tip and the sample ($\hat{\Sigma}_{TS}=\hat{T}_{TS}$, $\hat{\Sigma}_{ST}=\hat{T}_{ST}$, and $\hat{\Sigma}_{TT}=\hat{\Sigma}_{SS}=0$), and $\hat{g}^{+-}$ are the Green functions for the noninteracting case ($\hat{\Sigma}=0$), and are related to the density of states in the tip ($\hat{\rho}_{TT}$) and the sample ($\hat{\rho}_{SS}$) in the following way:

$$\hat{g}^{+-}_{TT}(\omega)=2\pi i\hat{\rho}_{TT}(\omega)f_T(\omega),$$
$$\hat{g}^{+-}_{SS}(\omega)=2\pi i\hat{\rho}_{SS}(\omega)f_S(\omega), \tag{9}$$
$$\hat{g}^{+-}_{ST}(\omega)=\hat{g}^{+-}_{TS}(\omega)=0,$$

where $f_{T,S}(\omega)$ are the Fermi-Dirac distributions for the tip and the sample, respectively.

We can obtain the retarded and advanced equilibrium Green functions for the interacting system from the usual Dyson equation using the Green functions of the uncoupled parts of the system, $\hat{g}^R$ and $\hat{g}^A$, and the interaction $\hat{\Sigma}$:

$$\hat{G}^R=\hat{g}^R+\hat{g}^R\hat{\Sigma}\hat{G}^R,\quad \hat{G}^A=\hat{g}^A+\hat{g}^A\hat{\Sigma}\hat{G}^A. \tag{10}$$

Using Eqs. (8), (9), and (10) we can write an expression for the tip-sample current that only involves the calculation of the Green functions for the uncoupled tip and sample and the hopping matrix that couples both parts of the system:

$$J=\frac{4\pi e}{\hbar}\int_{-\infty}^{\infty}\mathrm{Tr}\left[\hat{T}_{TS}\hat{\rho}_{SS}(\omega)\hat{D}^R_{SS}(\omega)\hat{T}_{ST}\hat{\rho}_{TT}(\omega)\hat{D}^A_{TT}(\omega)\right]\times[f_T(\omega)-f_S(\omega)]d\omega, \tag{11}$$

where

$$\hat{D}^R_{SS}(\omega)=[\hat{I}-\hat{T}_{ST}\hat{g}^R_{TT}(\omega)\hat{T}_{TS}\hat{g}^R_{SS}(\omega)]^{-1} \tag{12}$$

and

$$\hat{D}^A_{TT}(\omega)=[\hat{I}-\hat{T}_{TS}\hat{g}^A_{SS}(\omega)\hat{T}_{ST}\hat{g}^A_{TT}(\omega)]^{-1}. \tag{13}$$

These denominators take into account the multiple scattering effects via the summation up to infinity order of an expansion on the scattering matrices $\hat{X}^A=\hat{T}_{TS}\hat{g}^A_{SS}(\omega)\hat{T}_{ST}\hat{g}^A_{TT}(\omega)$ and $\hat{X}^R=\hat{T}_{ST}\hat{g}^R_{TT}(\omega)\hat{T}_{TS}\hat{g}^R_{SS}(\omega)$, and are responsible for the saturation of the tunneling current found when the distance between tip and sample becomes small.[5]

Equation (11) is our central result for the tunneling currents. This formula is not based in a perturbation theory expansion up to some given order, and therefore is valid even at small distances where multiple scattering effects become important, as discussed before. It includes more naturally temperature effects through the presence of the Fermi-Dirac distribution functions. Due to the high Fermi temperatures typical for metals, we expect the temperature dependence to be small at the usual experimental range (from 4 K to room temperature), and most easily incorporated in our formalism through the first term of an expansion around $T=0$ K.

We stress the following point: a correct evaluation of expression (11) should necessarily involve the calculation of the density of states associated with the tip and the sample and the corresponding Green functions. We take advantage here of the self-consistent linear combination of atomic orbitals (LCAO) formalism that we have previously developed to calculate the chemisorption of atoms on metallic or semiconducting surfaces. Therefore we can use the same Green functions calculated for the chemisorption problem to feed our Eq. (11). This makes a natural connection between the chemisorption and the STM problem, as we shall further discuss in the next section.

We also want to mention that expression (11) involves taking the trace of a multiplication of several matrices. This can physically be interpreted as a coherent superposition of different channels. Therefore, under appropriate conditions, interesting interference effects can be expected to appear.

As the last part of this introduction to our method for calculating the current between tip and sample, we want to show how the usual Tersoff-Hamann limit[6] can be obtained from the general expression (11). When the distance between

the tip and the sample is large enough, we can approximate the denominators $\hat{D}^A_{TT}(\omega)$ and $\hat{D}^R_{SS}(\omega)$ by the identity matrix to obtain the following expression for the current (valid when $\hat{T}_{TS}$ is small compared with the hopping interactions in the sample):

$$J \approx \frac{4\pi e}{\hbar}\int_{-\infty}^{\infty} \mathrm{Tr}[\hat{T}_{TS}\hat{\rho}_{SS}(\omega)\hat{T}_{ST}\hat{\rho}_{TT}(\omega)[f_T(\omega)-f_S(\omega)]d\omega. \tag{14}$$

In the limit of very low voltages (linear response regime) and zero temperature, we can simplify Eq. (14) and recover the Tersoff-Hamann expression for the tunneling current:

$$J \approx \frac{4\pi e^2 V}{\hbar}\mathrm{Tr}[\hat{T}_{TS}\hat{\rho}_{SS}(E_F)\hat{T}_{ST}\hat{\rho}_{TT}(E_F+eV)], \tag{15}$$

where V is the applied voltage and E_F is the Fermi level of the sample.

III. A FIRST-PRINCIPLES LCAO HAMILTONIAN FOR DESCRIBING THE TIP-SAMPLE COUPLING AND THE ADSORPTION OF XENON ON THE SAMPLE

To compute the required Green functions we have to solve the Hamiltonian for the uncoupled tip and sample systems. In both cases, we adopt a LCAO approach well suited for chemisorption problems; this method also affords the way for calculating $\hat{T}_{ST}$ in the Hamiltonian (2). Tight-binding methods have been introduced in the past as a convenient parametrization of the electronic properties of solids. However, these methods will encounter difficulties when quantities not closely related to the ones provided by the parametrization are required. To overcome this limitation, we have in our previous work[7] introduced a self-consistent tight-binding method, extending the Hohenberg-Kohn theorem[8] for a LCAO Hamiltonian.

In our formalism, we find it useful to analyze separately the one-electron and the many-body contributions to the sample Hamiltonian. Therefore we write the following equations:

$$\hat{H}_S = \hat{H}_S^{\mathrm{OE}} + \hat{H}_S^{\mathrm{MB}} \tag{16}$$

where

$$\hat{H}_S^{\mathrm{OE}} = \sum_{i\sigma} E_{i\sigma}\hat{n}_{i\sigma} + \sum_{ij;\sigma} T_{ij\sigma}(\hat{c}^\dagger_{i\sigma}\hat{c}_{j\sigma} + \hat{c}^\dagger_{j\sigma}\hat{c}_{i\sigma}) \tag{17}$$

defines the one-electron contribution and

$$\hat{H}_S^{\mathrm{MB}} = \sum_i U_i\hat{n}_{i\uparrow}\hat{n}_{i\downarrow} + \frac{1}{2}\sum_{i,j\neq i;\sigma}[J_{ij}\hat{n}_{i\sigma}\hat{n}_{j\sigma'} + \tilde{J}_{ij}\hat{n}_{i\sigma}\hat{n}_{j\sigma}] \tag{18}$$

defines the many-body part of the total Hamiltonian. In Eq. (17) E_i^σ represent the different orbital levels and T_{ij}^σ their hopping interactions. In Eq. (18), U_i, J_{ij}, and $\tilde{J}_{ij}$ are the intrasite and intersite Coulomb interactions between the orbital levels i and j. We can obtain the different values appearing in both equations from the Löwdin wave functions[9] of the system (ϕ_i); these wave functions are built using the atomic orbitals (ψ_i) by means of the general equation

$$\phi_i = \sum_j (S^{-1/2})_{ij}\psi_j \tag{19}$$

where S_{ij} is the overlap between the atomic orbitals i and j. It has been shown[10] that if we expand the orthogonal Löwdin orbitals up to second order in the overlap matrix, we can extract the different magnitudes that appear in the total Hamiltonian from the atomic wave functions of the sample;[11] this procedure has been shown to yield good results for most of the chemisorption problems we have analyzed. In particular, it has been demonstrated that the hopping interaction T_{ij} can be calculated using the Bardeen tunneling current between the atomic orbitals ψ_i and ψ_j:

$$T_{i,j} = -\frac{\gamma}{2}\int_{\sigma_{i,j}} dS(\psi_i\nabla\psi_j - \psi_j\nabla\psi_i) \tag{20}$$

with γ a coefficient that typically takes values between 1.3 and 1.5. Moreover, $E_{i\sigma}$ is shown to be the atomic level ϵ_i corrected by $-\Sigma_j S_{ij}T_{ij} + \frac{1}{4}\Sigma_j S_{ij}^2(E_i - E_j)$.

Solving the many-body part of Hamiltonian (16) is in general a difficult task. We have developed[7] a density functional approach to LCAO Hamiltonians like the one we are trying to solve. Using the Kohn-Sham approach, we solve in a self-consistent way the following effective one-electron Hamiltonian:

$$\hat{H}_S^{\mathrm{eff}} = \hat{H}_S^{\mathrm{OE}} + \sum_{i\sigma}[V^H_{i\sigma} + V^{\mathrm{XC}}_{i\sigma}]\hat{n}_{i\sigma}, \tag{21}$$

where $V^H_{i\sigma}$ and $V^{\mathrm{XC}}_{i\sigma}$ are the Hartree and exchange-correlation potentials associated with each orbital $i\sigma$:

$$V^H_{i\sigma} = \frac{\partial E^H[n_{i\sigma}]}{\partial n_{i\sigma}}, \quad V^{\mathrm{XC}}_{i\sigma} = \frac{\partial E^{\mathrm{XC}}[n_{i\sigma}]}{\partial n_{i\sigma}}, \tag{22}$$

with $n_{i\sigma}$ being the different occupation numbers. Much the same as in the Kohn-Sham approach, they must be obtained in a self-consistent way since the Hartree and exchange-correlation potentials depend on these values.

The Hartree potential can be written in a straightforward way:

$$V^H_{i\sigma} = U_i n_{i\bar{\sigma}} + \sum_{j\neq i;\sigma}[J_{ij}n_{j\bar{\sigma}} + \tilde{J}_{ij}n_{j\sigma}] \tag{23}$$

and it can be shown[12] that it is possible to find a functional dependence with the different occupation numbers $n_{i\sigma}$ for the exchange-correlation part of the Hamiltonian, E^{XC}, and define the exchange-correlation potential necessary to solve the Hamiltonian (21). In particular, a good approximation to the extra-atomic exchange-correlation energy (the main one contributing to the Xe physisorption energy) is given by

$$E^{\mathrm{XC}}[n_i] = -\frac{1}{2}\sum_{i\sigma}\alpha_i J_i n_{i\sigma}(1-n_{i\sigma}), \tag{24a}$$

where α_i is almost independent of $n_{i\sigma}$ and, J_i is the Coulomb interaction between one of the xenon electrons and the metal nearest-neighbor electrons. Then,

$$V^{\mathrm{XC}} = -\alpha_i J_i\left(\tfrac{1}{2} - n_{i\sigma}\right). \tag{24b}$$

The Hamiltonian (21) is solved self-consistently using Eqs. (22)–(24) for the many-body potentials. Once we calculate n_i from this solution we obtain the many-body energy using Eq. (24a), as well as the Hartree interaction between different charges.

It is important to notice that the effective one-electron Hamiltonian (21) defines the electronic properties of the system as a superposition of all the bonds i-j. This allows us to take a step further and analyze only the interaction between different independent subsystems. We have taken advantage of this feature to study the following. (i) First, we calculate the interaction of xenon and the metal, by assuming that the metal is well described by using some parameters taken from independent calculations.[19] This implies that our approach is focused on obtaining, as a first step, the adsorption energy for xenon on a metal surface. (ii) In a second step, we calculate the interaction between the tip (also described with some LCAO parameters taken from independent authors)[11] and the xenon-metal complex described by the solution of the problem analyzed in the first step. In this step, we assume $\hat{H}_T$ and $\hat{H}_S$ to be unperturbed and calculate $\hat{H}_I$ by means of Eq. (20).

The effective one-electron Hamiltonian (21) defines the electronic properties of the independent tip and sample. Thus we can calculate the Green functions needed for the evaluation of the current between tip and sample [Eq. (11)]:

$$\hat{g}^R_{SS}(\omega) = \frac{1}{(\omega + i\eta)\hat{I} - \hat{H}^{\mathrm{eff}}_S}, \quad \hat{g}^A_{SS}(\omega) = \frac{1}{(\omega - i\eta)\hat{I} - \hat{H}^{\mathrm{eff}}_S},$$

$$\hat{g}^R_{TT}(\omega) = \frac{1}{(\omega + i\eta)\hat{I} - \hat{H}^{\mathrm{eff}}_T},$$

$$\hat{g}^A_{TT}(\omega) = \frac{1}{(\omega - i\eta)\hat{I} - \hat{H}^{\mathrm{eff}}_T}, \tag{25}$$

where η is a positive constant close to zero.

The total-energy method that we have developed and successfully used on various systems[13] allows us to calculate the most favorable equilibrium position for the adsorption of xenon on the sample[14] and, subsequently, the tunneling currents between the tip and the sample with (or without) the xenon atom.

IV. METHOD OF CALCULATION OF THE TIP AND SAMPLE GREEN FUNCTIONS

The tip must be connected to a reservoir of electrons if a steady state has to be reached. This point has sometimes been overlooked in favor of models involving only atomic orbitals. Although we recognize the relevance of atomic orbitals in the explanation of important features for STM experiments, we also want to stress that electronic effects associated with the reservoir must be included in a realistic formalism. In our model, we provide such a reservoir by connecting a small cluster of atoms to a Bethe lattice with well-known electronic properties.

In all the calculations presented in this paper we have used the tip model shown in Fig. 1, with a cluster (C) of five atoms forming a pyramid having a base of four atoms. The atom at the apex of the pyramid yields most of the tunneling current defining the resolution of the microscope. In our model, each of the four atoms of the pyramidal base is joined to a Bethe lattice having the connection appropriate to the geometry of the metal tip. Other models with four atoms in the cluster with and without the atom at the apex have been considered previously,[15] where we have concluded that different tips can introduce changes in the calculations of the tunneling currents. Although this problem should be analyzed systematically considering different geometries, in this paper we concentrate on the particular case we have mentioned before for the sake of brevity.

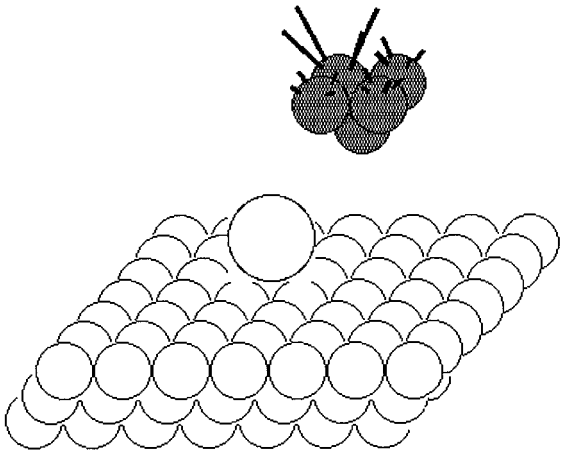

FIG. 1. Schematic view of the geometrical model for the tip-adsorbate-sample system. Last shell atoms in the cluster describing the tip are connected to a Bethe lattice with the appropriate coordination number.

We compute the electronic properties of the tip using a Green-function approach.[16] In this technique, the Bethe lattice is simulated by a self-energy matrix $\hat{\Sigma}_B$ that projects onto the four atoms of the pyramidal base the different Bethe lattices. This implies that the Green functions of the tip are given by the following equations:

$$\hat{g}^R_{TT}(\omega) = \frac{1}{(\omega + i\eta)\hat{I} - \hat{H}^{\mathrm{eff}}_C - \hat{\Sigma}^R_B(\omega)},$$

$$\hat{g}^A_{TT}(\omega) = \frac{1}{(\omega - i\eta)\hat{I} - \hat{H}^{\mathrm{eff}}_C - \hat{\Sigma}^A_B(\omega)}, \tag{26}$$

where $\hat{H}^{\mathrm{eff}}_C$ is defined by the LCAO Hamiltonian associated with the five-atom cluster of the tip, and $\hat{\Sigma}^{R(A)}_B(\omega)$ is the retarded (or advanced) self-energy of the Bethe lattice discussed above. Equation (26) replaces Eq. (25) for the tip, having introduced the Bethe lattice self-energy.

The effective one-electron Hamiltonian for the sample with (or without) the xenon atom is also solved using Green function techniques. In particular, the semi-infinite crystal is projected onto the last 12 layers, and the resulting film is joined to the adsorbed species. One of the advantages of using Green functions is that we can easily compute the

single-particle density of states associated with each orbital and their occupancies (we have already seen that these occupancies are required for self-consistent calculation of the xenon-sample interaction).

A simple way to get the two-dimensional Green function related to the surface is to project the bulk into the surface using techniques borrowed from renormalization group methods. In particular, to compute the needed Green functions we use a decimation technique for each $k_{\parallel}$ (Ref. 17) that is common to the chemisorption problem. The only disadvantage of this procedure is to have to deal with very big overlayer unit cells needed to describe isolated xenon atoms adsorbed on the sample. Our computational facilities limit us to the analysis of a 4×4 (Wood notation) overlayer at most, while the isolated xenon atom needs a 7×7 at least to be properly analyzed. Therefore for this 7×7 periodicity we have used a real-space approach where we describe the surface as a cluster formed by n shells.[18] This model yields all the Green function components $\hat{g}_{SS}$ needed to calculate the tunneling current.

V. RESULTS FOR THE PHYSISORPTION OF XENON ON THE SAMPLE SURFACE: Al AND Ni CASES

First of all we have analyzed the physisorption of xenon on two different metal surfaces, namely, Al(100) and Ni(100). Both cases present differences and similarities that are worthy of discussion.

Following the discussion presented in Sec. III, we have described the metal using conventional tight-binding parameters that are known to give a good description of the electron metal bands.[19] Then our method is applied to the calculation of the short-range interaction between the metal and xenon.

It is important to make a few comments about the atomic wave functions used for the metal atoms and xenon in our calculation. Regarding the metal, Al or Ni, we have used the single-ζ wave functions given by Clementi and Roetti:[11] core levels are treated as described in Ref. 20, while the valence electrons are analyzed in the LCAO approach discussed above. For xenon, the $5p$ and $6s$ levels define the valence electrons, while deeper levels are treated as the core levels of the metal. In this case, atomic wave functions are also taken from Ref. 11 except for the empty $6s$ state. We should comment that the use of this empty level as an atomic orbital contributing to the basic LCAO Hamiltonian is based on two independent pieces of evidence: first of all, previous STM calculations by Eigler, Weiss, Schweizer, and Lang[21] have shown that this $6s$ level yields an important contribution to the tunneling current crossing the xenon atom; on the other hand, Wandelt and Gumhalter[22] have also suggested, using qualitative models, the importance of that $6s$ level to the physisorption of xenon on the metal. Therefore we have obtained the xenon $6s$ level by means of a standard local density approximation (LDA) atomic calculation[23] that yields a $6s$ energy level located close to the vacuum level. Different interactions in Hamiltonian (1) are calculated from all these orbitals using standard programs available in the literature.[24]

The total xenon-metal potential is obtained by adding the short-range potential we have calculated to the van der Waals interaction:

$$V_{\mathrm{vdW}}\approx\frac{C_3}{(z-z_{\mathrm{vdW}})^3} \tag{27}$$

where z_{vdW} is the reference plane. Saturation effects are taken into account as discussed by Tang and Toennies,[25] and all the other parameters used in Eq. (27) are taken from well-known calculations found in the literature.[26]

We should also make a remark about the many-body potential used in Eq. (24b) for both xenon and the metal. In the last case, we have followed previous calculations[7] and taken $\alpha_i=1$; this includes most of the exchange-correlation effects. For xenon we have taken, however, $\alpha_i=1/2$; this yields the appropriate image potential for the empty $(6s)$ and the filled $(5p)$ atomic levels of xenon. This is checked by realizing that for the $6s$ level, $n_i\approx0$, while for the $5p$, $n_i\approx1$; then

$$V^{\mathrm{XC}}(6s)\approx-\tfrac{1}{4}J_i\,,\quad V^{\mathrm{XC}}(5p)\approx\tfrac{1}{4}J_i\,. \tag{28}$$

This shows that Eq. (28) yields the image potential for the $6s$ and $5p$ levels as it should.

We have analyzed the cases for xenon approaching the metal surfaces along three directions: center, bridge, and top sites. As we do not expect the metallic substrate to suffer significant reconstructions or even important relaxations, we have considered, for the sake of simplicity, a bulk-terminated structure for the substrate. Figure 2 shows (a) the Xe/Ni(100) and (b) the Xe/Al(100) interaction for xenon approaching the metal surface along the center position. In both cases, the minimum in the interaction energy appears for the center position due to the increase of the hybridization energy.[14] Figure 3 shows the short-range xenon-metal interaction split into its different contributions: kinetic (repulsive), hybridization, electrostatic, and exchange and correlation.[13]

It is worth noticing the attractive character of the short-range xenon-metal interaction (defined above). This is due to the role played by the $6s$ orbital which interacts with the metal very much as in a chemisorbed system; indicating that the $6s$ level is strongly broadened by the metal interaction, thus overlapping with the Fermi energy. Although this overlap is small (see Fig. 4), its effect is to increase substantially the hybridization contribution to the adsorption energy, yielding an atractive interaction.

The comparison between the Xe/Al(100) and the Xe/Ni(100) cases shows important differences associated mainly with the equilibrium distance for the xenon-physisorbed potential. While for Al we find that xenon is located at 4.6 Å from the metal layer, for Ni we find this distance to be reduced to 3.3 Å. This difference can be explained by the different density of states that Al and Ni have for the s electrons at the Fermi level. Al has a very high density of s electrons that yield a strong repulsion with the occupied xenon levels. For Ni, this density is much smaller and the Ni-Xe repulsion is not strong enough until the Ni d electrons start to interact with xenon. This explains why xenon penetrates 1.3 Å deeper in the case of Xe/Ni(100) than that of Xe/Al(100). These results are relevant from the STM point of view, since xenon atoms can be expected to show a larger corrugation when deposited on Al.

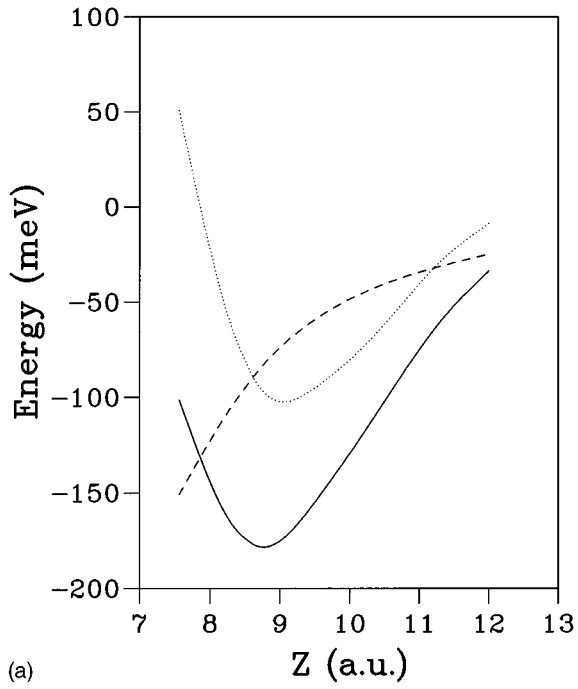

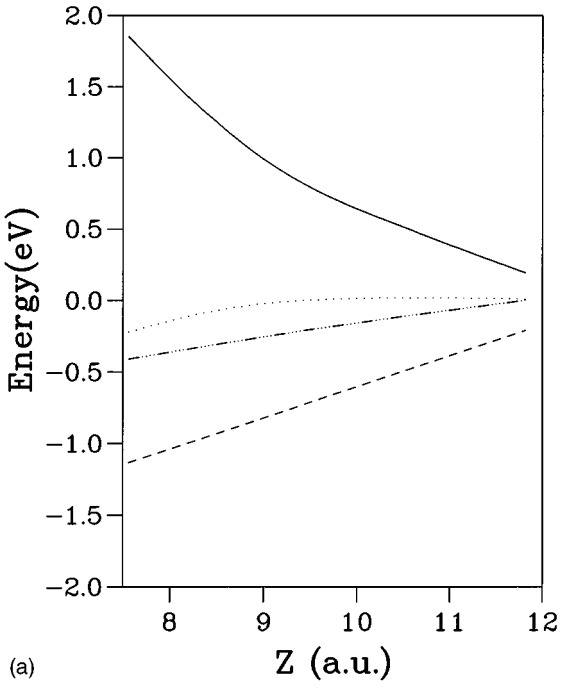

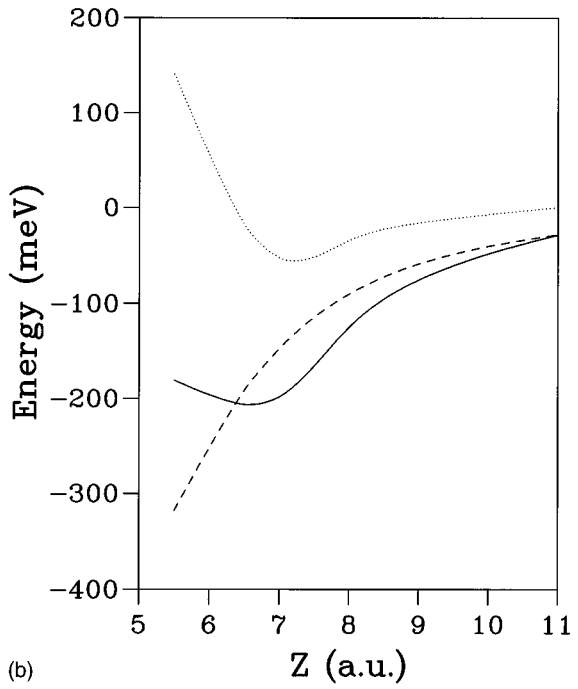

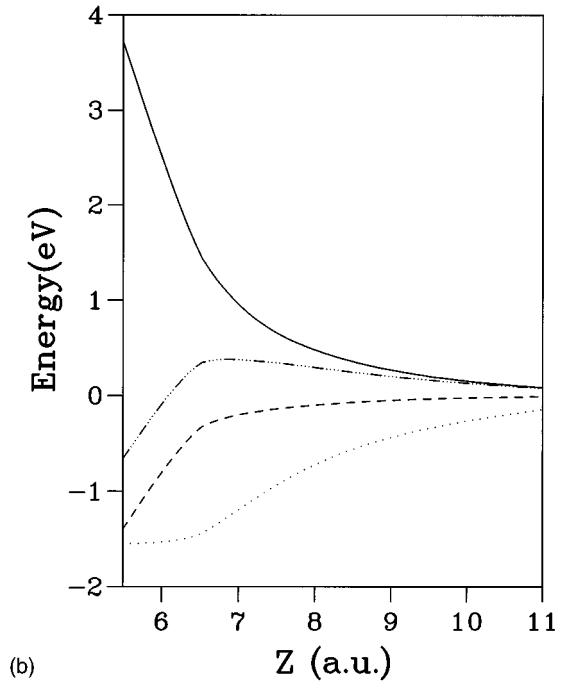

FIG. 2. Adsorption energies for (a) Xe/Al(100) and (b) Xe/Ni(100). Different contributions to the total adsorption well (full line) are short-range (dotted line) and long-range (dashed line).

FIG. 3. Different contributions to the short-range interaction: (i) kinetic (solid line), (ii) hybridization (dashed), (iii) electrostatic (dotted), and (iv) exchange-correlation (dashed dotted). (a) Xe/Al(100) and (b) Xe/Ni(100).

VI. TUNNELING CURRENTS: CORRUGATION AND CONDUCTANCE

In this section we analyze the tunneling currents and the associated corrugations for a given tip-sample configuration, with and without a xenon atom adsorbed on the surface. First of all, we consider the clean Al(100) and Ni(100) surfaces, and their interaction with different tips. Atomic resolution images of clean metal surfaces[27] have attracted a great deal of attention, and the mechanisms by which they are observed are still under debate.[28] As discussed below, our model can easily explain corrugations below 0.2 Å for the usual tunneling conditions. For extreme conditions, i.e., near the close contact regime, we find inverted images for Al-like tips, with a significant increase in corrugation by about a factor of 2. These numbers still fall short by approximately the same factor to explain values reported in the literature as big as 0.8 Å. But under these conditions the experimental situation is not clear at all. This regime has been discussed in terms of physical contact, and therefore involves important experi-

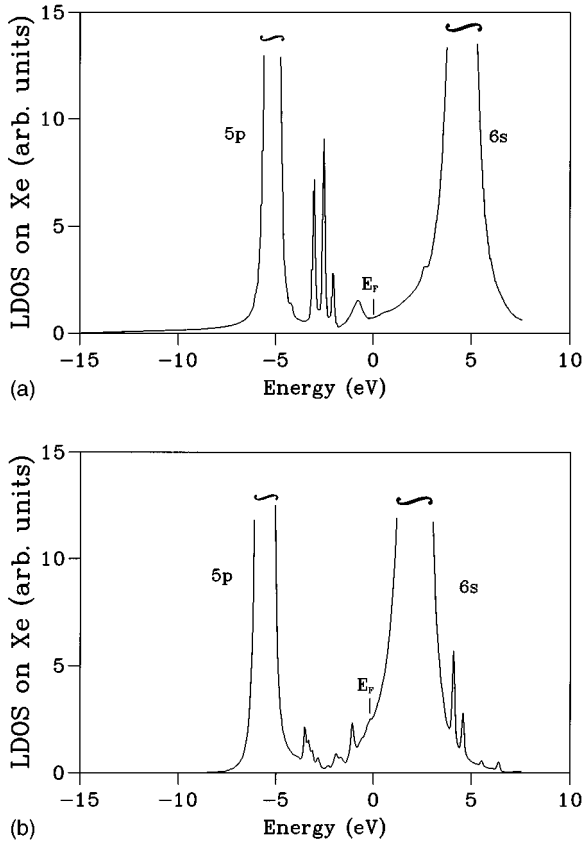

FIG. 4. Local density of states on xenon orbitals. (a) Xe/Al(100) and (b) Xe/Ni(100).

mental complications. However, from a theoretical point of view, that limit is still quite realistically described in our formalism, which includes the relevant physics here: current saturation via multiple-scattering effects, and possibly the formation of new chemical bonding, taken into account via a hopping matrix. Finally, we proceed to analyze similar cases with xenon adsorbed on the metal, using the information we have discussed in the previous section.

A. Clean Al(100) and Ni(100) surfaces

Al and Ni tips have been considered. As discussed in Sec. IV, it has been assumed that the tip is represented by a pyramidal cluster of five atoms. Ni tips can be prepared currently. Although Al tips cannot be treated in similar ways, one can expect the formation of a quasiconventional Al tip via the mechanical contact of another kind of tip (Ni, W, etc.) with an Al surface, resulting in a group of Al atoms gathered at the apex of the tip.

1. Aluminum tip

We find a similar behavior regarding tunneling currents for the Al(100) and Ni(100) surfaces. In general, for distances between the the tip and the sample larger than 2.8 Å for Al(100) and 2 Å for Ni(100), the conductance reaches the highest value when the tip is located above the surface atoms (Fig. 5), giving images with normal corrugation. From Fig. 5, we obtain that the amplitude of this normal corrugation is about 0.1 Å and 0.2 Å for Al(100) and Ni(100), respectively.

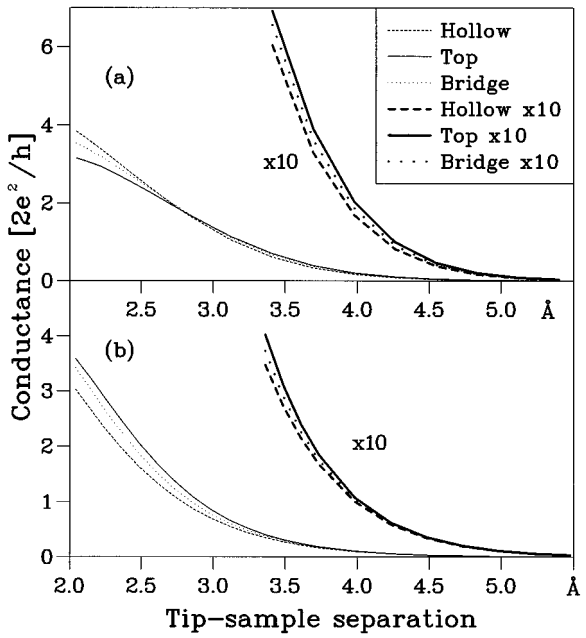

FIG. 5. Conductance versus tip-sample separation for an aluminum tip on (a) Al(100) and (b) Ni(100).

For smaller distances between the tip and the sample, the conductance above the surface atoms becomes lower than above the bridge and the hollow sites for aluminum and, as a consequence, the corrugation becomes inverted. The behavior of the tunneling current presented in Fig. 5 is related to the different orbitals of the apex atom: s and p_z orbitals control the current from the surface region located directly below the tip, contributing in this way to the normal corrugation (the p_z orbital is oriented perpendicularly to the surface). The contributions of these orbitals dominate over larger distances, which leads to the normal corrugation of the total current. On the other hand, for very small distances the s and p_z contributions saturate and then the p_x and p_y contributions become dominant. As these orbitals are oriented parallel to the surface, their relative contributions are maximized when the tip is located above the empty sites of the two-dimensional (2D) unit cell, leading to the inverted corrugation.

2. Nickel tip

When $d>5.5$ Å for Al(100), or $d>3.5$ Å for Ni(100) (Fig. 6), we find that the nickel tip does not give any appreciable corrugation. Under these conditions, the conductance does not change when scanning the surface, and STM images are flat. For a smaller separation, the Ni(100) surface gives images with the normal corrugation. This normal corrugation is caused by the d orbitals of the apex atom giving the strongest contribution to the tunneling current when $d<2.5$ Å. The Al(100) case is quite similar. As before, for small distances the most important current contributions are related to the d orbitals, but the behavior of the tunneling current is now somewhat more complicated. For 2.5 Å $<d<5.5$ Å the largest and the lowest conductances appear above the hollow points and above the surface atoms, respectively, and the corrugation appears inverted (with an amplitude below 0.1 Å). But for $d<2.5$ Å the lowest conductance appears above

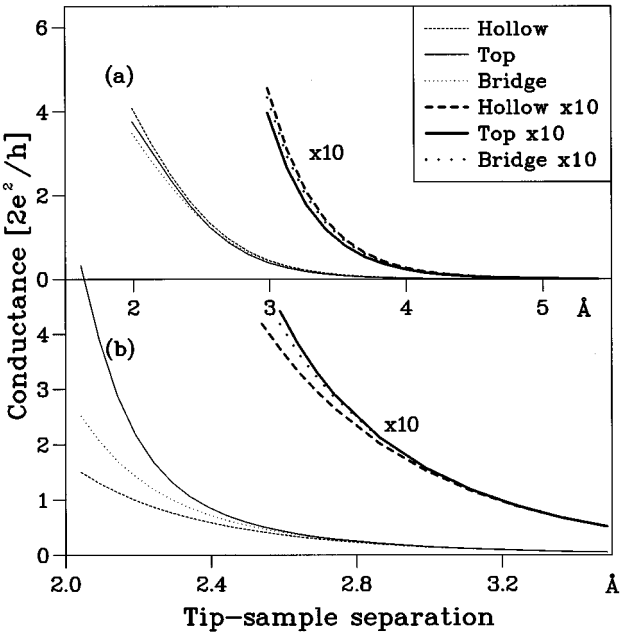

FIG. 6. Conductance versus tip-sample separation for a nickel tip on (a) Al(100) and (b) Ni(100).

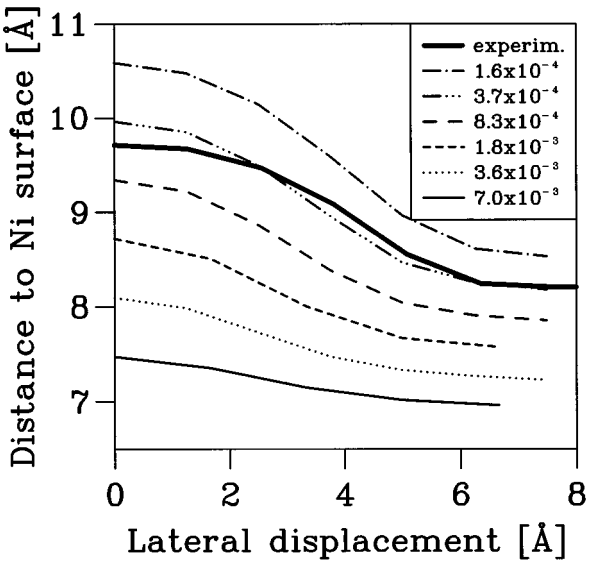

FIG. 7. W tip, isolated xenon atom on Ni(100): theoretical scannings at different conductances (in units of the quantum of conductance) are shown along with the experimental result from Eigler *et al.* (full line).

the bridge points; then the evolution of the conductance along the surface shows two types of maxima, the higher one happening above the hollow sites, and the smaller one appearing above the surface atoms. Both are due to contributions from the *d* orbitals. It should be noted that, contrary to the Al tip, the *s* orbital of the apex atom does not contribute too much to the normal corrugation. This is due to the larger radius of the *s* orbital in the Ni atom (compared with Al). From these results, we conclude that the *d* orbitals of the apex atom control the tunneling current only for very small tip-sample distances ($d<2.8$ Å). These contributions disappear quickly when *d* increases, and because other orbitals of the Ni tip in practice do not contribute to the total corrugation, the images of Al(100) and Ni(100) surfaces, obtained with the Ni tip, are flat for greater distances.

In general, our calculations show that the atomic resolution of STM images for clean metal surfaces depends considerably on the electronic structure of the tip. The images of the same surface obtained with different tips may look very different and present even opposite kinds of corrugation (normal or inverted) depending on the sample-tip distance. This conclusion also suggests that the tip geometry must be important for the atomic resolution operation of the microscope.[15,29]

B. Xe-covered Al(100) and Ni(100) surfaces

Using our theoretical results for the deposition of xenon on Al or Ni, we analyze in this section their STM tunneling currents. Two different cases will be discussed: (i) isolated xenon atoms and (ii) a 2×2 xenon overlayer.

1. Isolated xenon atoms

For this case, in order to have a good resolution of the isolated xenon atom, at least a 7×7 overlayer periodicity has to be used. This long periodicity guarantees that xenon atoms do not interfere with each other.

In our calculations, however, we have used the real-space Green function method (discussed in Sec. IV), which considers a single xenon atom adsorbed on a cluster having 50 atoms on the surface and three layers. Regarding the tip, we have computed its Green function following the technique also discussed in Sec. IV.

Following this procedure we have calculated, first of all, a constant-current STM image for the Xe/Ni(100) system. The tip-sample separation has been chosen to yield the same tunneling current as in the experiments of Eigler *et al.*[21] (4×10^{-4} in units of the quantum of conductance $2e^2/h$; notice that the inverse is approximately 11 KΩ). Figure 7 shows our results for a W tip compared with the experiments: we find that the tip is located around 9.0 Å above the metal layer, and that the width of the corrugation signal is large, around two lattice parameters, in good agreement with the experimental evidence. In this particular case we have modeled the tip by a single W atom attached to an appropriate Bethe lattice. These results already show that xenon atoms can only be observed individually if they are not located too close to each other. Notice also that the apparent corrugation of xenon is 1.8 Å while the adsorption distance of xenon to Ni(100) is calculated to be 3.4 Å. This is due to a smaller Fermi level density of states on the xenon atom, mainly associated with the 6*s* orbital, than on the Ni surface atoms, by almost two orders of magnitude. Figure 7 also shows different corrugation curves for different conductances, around the value of 4×10^{-4} considered before. As clearly seen in this figure, the corrugation increases with decreasing conductance: this is related to the fact that at larger tip-sample distances the tip selects with a larger weight the density of states associated with the xenon 6*s* orbital, with respect to the metal.

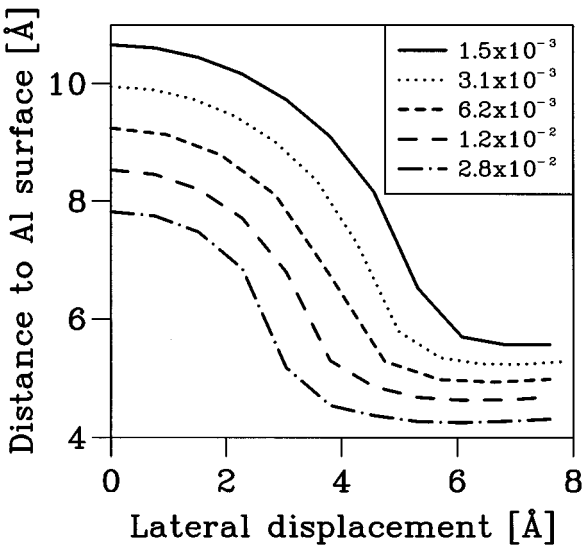

FIG. 8. W tip, isolated xenon atom on Al(100): theoretical scannings at different conductances (in units of the quantum of conductance) are shown.

Following the same approach we have also calculated the STM image of a xenon atom adsorbed on Al(100), as seen by a W tip. Taking the height calculated above, we obtain the corrugation signal shown in Fig. 8. The maximum corrugation obtained from Fig. 8 is around 4.5 Å. Notice how this value is quite similar to the adsorption distance on this substrate, unlike the Xe/Ni(100) case. This is a consequence of the electronic properties of the system: in this particular case the densities of states on the Al and xenon atoms are more alike than before and the contribution of the aluminum atoms to the total tunneling currents is not large enough to decrease the corrugation associated with an isolated xenon atom.

2. Xe 2×2 adsorbed layer

In general, contrary to the single-atom case discussed above, the STM images of the 2×2 adsorbed layer depend considerably on the electronic properties of the tip. We have found important differences between the behavior of the tunneling currents obtained with aluminum and nickel or platinum tips.

a. Aluminum tip. For this tip and for tip-sample distances of around 9.0 Å , the xenon overlayer shows a normal corrugation[30] with an amplitude of 0.5 Å. For smaller tip-sample distances ($d\leqslant8.3$ Å), the corrugation for the xenon overlayer appears inverted, with the tunneling current reaching a maximum either in the bridge or in the hollow sites.

These results can be understood in terms of the tunneling currents across each individual atom. Figure 9 shows the single Xe/Al(100) conductance for a constant tip (Al)–sample distance of 8.95 Å. Two different scans (over the bridge and the hollow positions, respectively) obtained by superimposing isolated xenon atom images are shown in the same figure to mimic the profile of the 2×2 overlayer.

The result shows that the image of the 2×2 overlayer can be obtained by overlapping the signals of the different individual atoms.

b. Nickel tip. This tip yields a broader signal for the xenon corrugation than an aluminum tip. Figure 10 shows the

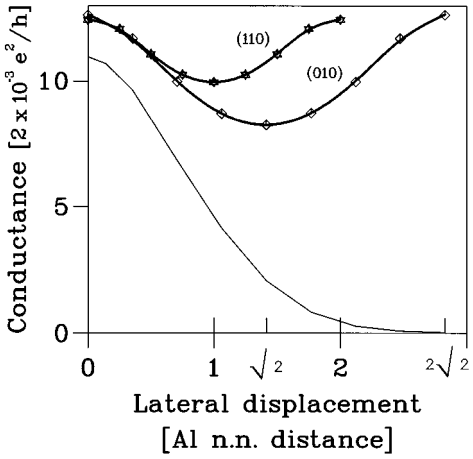

FIG. 9. Constant distance (8.95 Å) scanning with an aluminum tip (lateral displacement is given in units of the substrate nearest-neighbor distance) for a single xenon atom adsorbed on Al(100). The two upper curves are obtained superimposing isolated atoms, to simulate a scan of a 2×2 xenon overlayer along two different directions; (110) and (010).

Xe/Al(100) corrugation for a single xenon atom and different tip-sample distances. Comparison with Fig. 9 shows that this signal is broader than the one obtained with an aluminum tip. This is mainly the result of the nickel *d* orbitals. They interact not only with the atoms located on the direction perpendicular to the surface but also with other xenon atoms.

Due to the broad signal found for the nickel tip for a tip-sample distance of 9.0 Å (similar results are also found for a platinum tip), the xenon 2×2 overlayer presents an inverted corrugation of 0.3 Å. This result can also be deduced independently by overlapping the individual signals coming from each xenon atom. A normal corrugation can only be obtained with a nickel tip if we go to larger tip-sample distances.

We conclude that corrugations of individual atoms and ordered layers depend on the tip used to scan the surface.[29] Transition metal tips yield broader corrugation signals than normal metal tips, and can present, in some cases, inverted corrugations. Our results also show that the corrugation signal of a xenon ordered layer can be calculated by adding the currents associated with each independent atom. This result

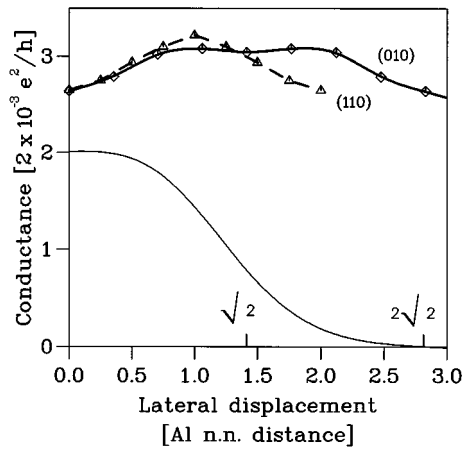

FIG. 10. Same as Fig. 9 with a nickel tip.

depends mainly on the possibility of neglecting the interference between the currents associated with different adsorbed atoms: this has been found to be the case for the xenon atoms in a 2×2 ordered layer. In general, we can expect this result to be valid if the adsorbed atoms are not too much closer: our results show that this is always the case if the adsorbed atoms are not located on the nearest-neighbor sites of the surface unit cell (details will be published elsewhere).

VII. CONCLUSIONS

In this paper we have presented a self-consistent LCAO method that treats on the same footing both the properties of chemisorbed species and the tunneling currents for the scanning tunneling microscope.[7]

Self-consistent LCAO Hamiltonians for chemisorption problems have been analyzed elsewhere. In this approach a local density approximation, whereby many-body effects are introduced by means of a local potential associated with each atomic orbital, is crucial and establishes the formal equivalence between tight-binding Hamiltonians and conventional LDA methods. This approach also yields the means to compute the coupling between the two sides (tip and sample) of the interface of a scanning tunneling microscope. The link between LCAO methods and the calculation of tunneling currents is provided by the Bardeen matrix element given by Eq. (20).[31] This coupling defines the interaction Hamiltonian between the tip and the sample and allows us, using the Keldysh method described in Sec. II, to calculate the tunneling currents for the microscope.

In this paper we have also applied the previous approach to the calculation of (i) the physisorption of xenon on different metals and (ii) the tunneling currents associated with the adsorbed xenon atoms. This study has allowed us to apply our theoretical approach in its full power, obtaining the chemisorption (or physisorption) properties of the adsorbed xenon and the tunneling currents for different tips and tip-sample distances. The advantage of this system studied is that there is some experimental evidence to check our theoretical results. Regarding this point, it is very satisfactory that our calculations for the tunneling currents and the surface corrugation of xenon on Ni(100) show a remarkable agreement with the experimental data.[21] It is also important to notice that the corrugation of a single xenon atom is deeply related to its position with respect to the metal surface. This suggests that the Xe-Ni distance, as obtained in our calculation (≈3.3 Å), can be taken very confidently. In this regard, notice that a change of 0.5 Å in the Xe-Ni distance will be reflected in a change of around 0.3 Å in the xenon corrugation.

Finally, we have also explored the effects of different tips on the corrugation of a single xenon atom and a xenon 2×2 overlayer. In general, we have found that different metal tips can change the xenon corrugation and modify the STM images depending on the distance and the surface geometry.[29] These results indicate that STM images should be analyzed by comparing iteratively theory and experiment, very much in the same way as it is usually done for other surface sensitive techniques, like low-energy electron diffraction (LEED), photoelectron diffraction, surface-extended x-ray-absorption fine structure (SEXAFS), etc.

ACKNOWLEDGMENTS

We acknowledge financial support from the Spanish CICYT under Contracts No. PB92-168C and No. PB91-930, and from the European Community, EC(CHRX-C793-0134). Iberdrola S. A. is gratefully acknowledged for help and encouragement.

*On leave of absence from Institute of Experimental Physics, University of Wrocław, Cybulskiego 36, P-50-205 Wrocław, Poland.

†Present address: Condensed Matter Theory Group, The Blackett Laboratory, Imperial College, London SW7 2BZ, U.K.

[1] G. Binnig, F. Fuchs, Ch. Gerber, H. Rohrer, E. Stoll, and E. Tosatti, Europhys. Lett. **1**, 31 (1986).

[2] L.V. Keldysh, Zh. Eskp. Teor. Phys. **47**, 1515 (1964) [Sov. Phys. JETP **20**, 1018 (1965)].

[3] J. Bardeen, Phys. Rev. Lett. **6**, 57 (1961).

[4] C. Caroli, R. Combescot, P. Nozieres, and D. Saint-James, J. Phys. C **4**, 916 (1971); A. Martin-Rodero, F. Flores, and N.H. March, Phys. Rev. B **38**, 10 047 (1988).

[5] N.D. Lang, Phys. Rev. B **36**, 8173 (1987); J. Ferrer, A. Martin-Rodero, and F. Flores, *ibid.* **38**, 10 113 (1988).

[6] J. Tersoff and D.R. Hamann, Phys. Rev. Lett. **50**, 1998 (1983); Phys. Rev. B **31**, 805 (1985).

[7] F.J. Garcia-Vidal, J. Merino, R. Perez, R. Rincon, J. Ortega, and F. Flores, Phys. Rev. B **50**, 10 537 (1994).

[8] P. Hohenberg and W. Kohn, Phys. Rev. **136**, 864 (1964).

[9] P.-O. Löwdin, J. Chem. Phys. **18**, 365 (1950).

[10] F.J. Garcia-Vidal, A. Martin-Rodero, F. Flores, J. Ortega, and R. Perez, Phys. Rev. B **44**, 11 412 (1991).

[11] E. Clementi and C. Roetti, At. Data Nucl. Data Tables **14**, 177 (1974).

[12] F. Flores, R. Saiz-Pardo, R. Rincon, J. Ortega, and F.J. Garcia-Vidal, J. Phys. Condens. Matter **5**, A41 (1993).

[13] This method has been successfully applied on semiconductor surfaces too: e.g., see R. Rincon, F.J. Garcia-Vidal, and F. Flores, Surf. Sci. **320**, 297 (1995); F. Flores, F.J. Garcia-Vidal, and R. Perez, Philos. Mag. **69**, 931 (1994).

[14] R. Perez, F.J. Garcia-Vidal, P.L. de Andres, and F. Flores, Surf. Sci. **307/309**, 704 (1994).

[15] J.R. Cerda, P.L. de Andres, F. Flores, and R. Perez, Phys. Rev. B **45**, 8721 (1992).

[16] L. Martin-Moreno and J.A. Verges, Phys. Rev. B **42**, 7193 (1990).

[17] F. Guinea, C. Tejedor, F. Flores, and E. Louis, Phys. Rev. B **28**, 4397 (1983).

[18] Shi-Yu Wu and Chakram S. Jayanthi, Int. J. Mod. Phys. B **9**, 1869 (1995).

[19] D.A. Papaconstantopoulos, *Handbook of the Band Structure of the Elemental Solids* (Plenum, New York 1986).

[20] E.C. Goldberg, A. Martin-Rodero, R. Monreal, and F. Flores, Phys. Rev. B **39**, 5684 (1989).

[21] D.M. Eigler, P.S. Weiss, E.K. Schweizer, and N.D. Lang, Phys. Rev. Lett. **66**, 1189 (1991).

[22] K. Wandelt and B. Gumhalter, Surf. Sci. **140**, 355 (1980).
[23] D.R. Hamann, M. Schluter, and C. Chiang, Phys. Rev. Lett. **43**, 1494 (1979); S.G. Louie, S. Froyen, and M.L. Cohen, Phys. Rev. B **26**, 1738 (1982).
[24] J. Fernandez Rico, R. Lopez, and G. Ramirez, Stud. Phys. Theor. Chem. **77**, 241 (1992); J. Comput. Chem. **9**, 790 (1988).
[25] K.T. Tang and J. Peter Toennies, Surf. Sci. **279**, L203 (1992).
[26] C. Schwartz and R.J. Le Roy, Surf. Sci. **166**, L141 (1986).
[27] V.M. Hallmark, S. Chiang, J.F. Rabolt, J.D. Swalen, and R.J. Wilson, Phys. Rev. Lett. **59**, 2879 (1987); J. Wintterlin, J. Wiechers, H. Brune, T. Gritsh, H. Höfer, and R.J. Behm, *ibid.* **62**, 59 (1989).
[28] H. Sirringhaus, E.Y. Lee, and H. von Känel, Phys. Rev. Lett. **74**, 3999 (1995).
[29] S. Watanabe, M. Aono, and M. Tsukada, Appl. Surf. Sci. **60/61**, 437 (1992).
[30] F. Flores, P.L. de Andres, F.J. Garcia-Vidal, L. Jurczyszyn, N. Mingo, and R. Perez, Prog. Surf. Sci. **48**, 27 (1995).
[31] C. Julian Chen, Phys. Rev. Lett. **69**, 1656 (1992).